ChemComm

View Online
Dynamic Article Links

Cite this: *Chem. Commun.*, 2011, **47**, 6075–6077

www.rsc.org/chemcomm

COMMUNICATION

Butylphenyl-functionalized palladium nanoparticles as effective catalysts for the electrooxidation of formic acid†

Zhi-You Zhou,[ab] Xiongwu Kang,[a] Yang Song[a] and Shaowei Chen*[a]

Received 2nd March 2011, Accepted 8th April 2011
DOI: 10.1039/c1cc11235j

Monodisperse butylphenyl-functionalized palladium (Pd-BP, dia. 2.24 nm) nanoparticles were synthesized through co-reduction of butylphenyldiazonium and H_2PdCl_4 by $NaBH_4$. Because of this unique surface functionalization and a high specific electrochemical surface area (122 m^2 g^{-1}), the Pd-BP nanoparticles exhibited a mass activity ~4.5 times that of commercial Pd black for HCOOH electrooxidation.

Direct formic acid fuel cells (DFAFCs) are a promising power source for portable electronic devices due to their high energy density, modest operating conditions, relatively low toxicity and the low crossover rate of formic acid through Nafion membranes.[1–5] The anodic reaction of DFAFCs is formic acid electrooxidation to CO_2 on Pt- or Pd-based catalysts. Pt catalysts typically exhibit a high intrinsic activity. However, they are vulnerable to surface poisoning by adsorbed CO (CO_{ad}), a reaction intermediate.[6,7] In contrast, Pd is free of CO_{ad} poisoning in the short term, and formic acid is mainly oxidized *via* the direct pathway.[8,9] Yet, the electrooxidation of HCOOH on Pd catalysts in general requires a substantially high overpotential (~0.3 V), which significantly impedes the large-scale commercialization of DFAFCs.

To improve the catalytic activity, especially the activity per mass of precious metals, one key issue is to rationally control the size and nature of surface structures, such as crystalline planes and surface ligands, of nanoparticle catalysts.[10–12] Previously, we have synthesized Pd nanoparticles through palladium–carbon covalent linkages by using diazonium derivatives as the functional ligands and controlling the particle core size at 2.4–3.6 nm by varying the ratio of Pd precursors to the diazonium salts.[13] In this communication, we prepared butylphenyl-stabilized palladium (Pd-BP) nanoparticles (dia. 2.24 nm) by a modified procedure. The resulting particles exhibited a mass activity (3.39 A mg^{-1}_{Pd}) that was the best among the pure Pd catalysts known so far for formic acid electrooxidation. Additionally, the peak potential of formic acid electrooxidation showed a negative shift of *ca.* 80 mV, in comparison to that of a commercial Pd catalyst.

The Pd-BP nanoparticles were synthesized by co-reduction of H_2PdCl_4 and butylphenyldiazonium (see ESI† for details). Briefly, the diazonium salt was synthesized from a stoichiometric amount of 4-butylaniline (1 mmol) and sodium nitrite in ice-cold 50 wt% fluoroboric acid.[14] In comparison with the previous synthetic method,[13] one major modification in the present study is the employment of a toluene–THF solvent instead of toluene alone. In the mixed solvent, both the diazonium salt and H_2PdCl_4 can be readily dissolved and co-reduced by $NaBH_4$, without a phase transfer procedure (see ESI† for details).

The morphology of the Pd-BP nanoparticles was first characterized by transmission electron microscopy (TEM, JEOL-1230 at 120 kV). Fig. 1a shows a representative TEM image of the as-prepared Pd-BP nanoparticles. A uniform and well-dispersed film of nanoparticles can be observed. The average core size of the Pd nanoparticles is 2.24 nm, with a relative standard deviation of 16% (Fig. 1b). In contrast, commercial Pd black exhibited a much larger particle size (*ca.* 10 nm), along with a number of particle aggregates (Figs 1c and d), consistent with previous TEM results.[8]

We then carried out FTIR spectroscopic measurements (using a Perkin-Elmer Spectrum One FTIR spectrometer) to characterize the surface ligands on the Pd-BP nanoparticles. The IR samples were prepared by dropcasting a concentrated solution of Pd-BP in toluene onto a NaCl disk. After solvent evaporation, a uniform film of nanoparticles was formed. From the FTIR spectrum of the Pd-BP nanoparticles (curve A) depicted in Fig. 2a, one can see that in the C–H stretching vibration region (2700–3100 cm^{-1}), the band at 3027 cm^{-1} can be assigned to the C–H stretch of the aromatic ring, and the two coupled bands to the C–H stretches of CH_3 (ν_{as} = 2955 cm^{-1}, and ν_s = 2869 cm^{-1}) and CH_2 (ν_{as} = 2926 cm^{-1}, and ν_s = 2855 cm^{-1}). The aromatic ring skeleton vibrations can be identified by the four bands at 1614 (a very weak shoulder peak, indicated by an arrow), 1584, 1497, and 1463 cm^{-1}.[15] In addition, the weak band at 827 cm^{-1} is the characteristic peak of a *para*-substituted aromatic ring (with an out-of-plane C–H deformation vibration).[15] These infrared characteristics demonstrate that the ligands on the Pd-BP surface are indeed the butylphenyl fragments by virtue of the Pd–C interfacial covalent linkage.[13] We note that the relative intensities of the

[a] *Department of Chemistry and Biochemistry, University of California, 1156 High Street, Santa Cruz, California 95064, USA. E-mail: shaowei@ucsc.edu*
[b] *State Key Laboratory of Physical Chemistry of Solid Surfaces, Department of Chemistry, Xiamen University, Xiamen 361005, CHINA*

† Electronic supplementary information (ESI) available: Detailed synthetic procedures. See DOI: 10.1039/c1cc11235j

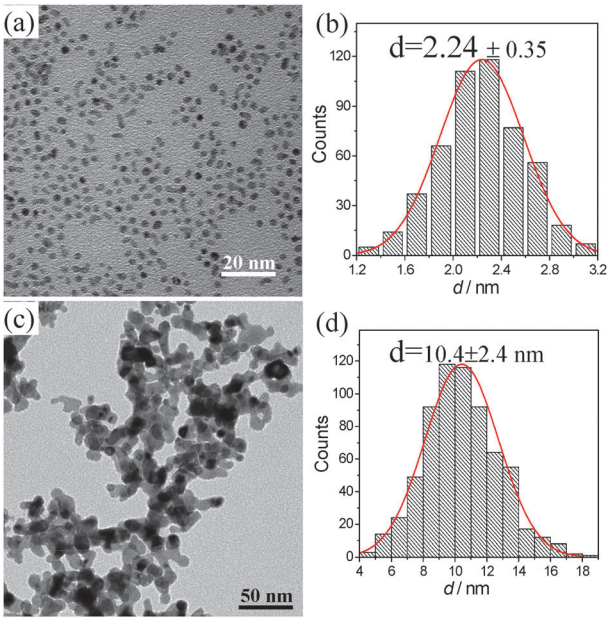

Fig. 1 TEM images and core size histograms of (a, b) Pd-BP nanoparticles and (c, d) commercial Pd black. Note that large aggregates in the Pd black sample are excluded in the size analysis.

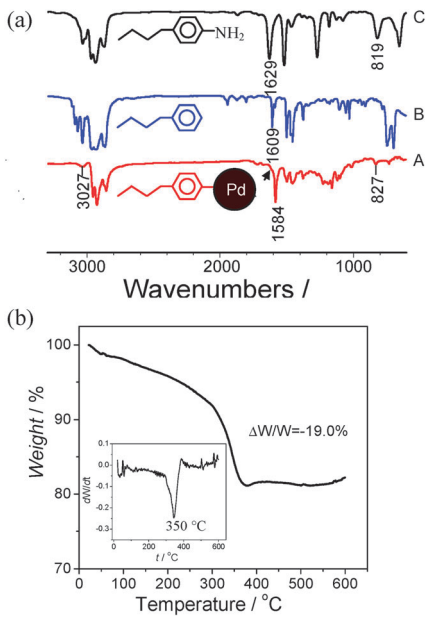

Fig. 2 (a) FTIR spectra of (A) the Pd-BP nanoparticles, (B) *n*-butyl benzene, and (C) 4-butylaniline. (b) The TGA curve of the Pd-BP nanoparticles measured under a N_2 atmosphere at a heating rate of 10 °C min^{-1}. The inset shows the derivative of the TGA curve, showing the weight loss peak at 350 °C.

aromatic ring skeleton vibrations of the butylphenyl groups bound onto the Pd nanoparticles are significantly different from those of free *n*-butylbenzene and 4-butylaniline (curves B and C). For instance, the strong band observed with monomeric *n*-butylbenzene at 1609 cm^{-1} and with 4-butylaniline at 1629 cm^{-1} became a very weak shoulder with Pd-BP, whereas the 1584 cm^{-1} band markedly intensified with the ligands bound onto the nanoparticle surface. These observations suggest that the Pd-BP nanoparticles were free of excessive ligands and relatively strong electronic interactions occurred between the aromatic rings and the Pd nanoparticles.

Thermogravimetric analysis (TGA, using a Perkin-Elmer Pyris 1Thermogravimetric Analyzer) was then performed to quantify the number of ligands on the Pd-BP nanoparticles. As shown in Fig. 2b, the weight loss started quickly after 300 °C, yielding a peak at 350 °C (inset of Fig. 2b). At temperatures higher than 375 °C, the mass of the sample remained almost constant and the total weight loss was about 19%. On the basis of the weight loss and the average core size of the Pd nanoparticles, we can estimate that the average area occupied by one butylphenyl ligand is about 21 $Å^2$, which is close to the typical value (~20 $Å^2$) for long-chain alkanethiolates adsorbed on metal surfaces.[16]

The catalytic activity of the Pd-BP nanoparticles in the electrooxidation of formic acid was then examined by voltammetric measurements. Electrochemical studies were carried out in a standard three-electrode cell connected to a CHI-440 electrochemical workstation, with a Pt foil counter electrode and a saturated calomel electrode (SCE) at room temperature. To prepare the working electrode, a calculated amount of a Pd-BP nanoparticle solution in toluene was dropcast onto a polished glassy carbon (GC, ϕ = 5 mm) electrode. As soon as the electrode was dried in air, a dilute Nafion solution (0.1 wt%, 2 μL) was added onto it. A commercial Pd catalyst (Aldrich) was loaded onto the GC electrode surface in a similar fashion and employed as a benchmark material for comparison.

Fig. 3a shows the cyclic voltammograms of Pd-BP and commercial Pd black in 0.1 M H_2SO_4. The currents have been normalized to the mass loadings of Pd. Unlike conventional surface-capping reagents, such as PVP, that bind strongly onto the nanoparticles and significantly diminish the accessibility of the nanoparticle surface,[17] the surface of Pd-BP is fairly accessible for electrochemical reactions, and only 2 to 3 potential cycles are needed to produce a stable voltammetric profile. In Fig. 3a, the current between −0.25 and 0.0 V can be ascribed to the adsorption/desorption of hydrogen and (bi)sulfate on the Pd surfaces, as well as absorption of a small fraction of hydrogen into the Pd lattice.[18–20] A well-defined cathodic peak at around +0.30 V can be observed which is assigned to the reduction of Pd oxide that was formed in the positive potential scan. Woods *et al.*[21] have reported that a monolayer of Pd oxide would form on the Pd surface at +1.50 V (RHE), which is a value equal to +1.20 V (SCE) in 0.1 M H_2SO_4 in the present study, and the reduction of the Pd oxide corresponds to a charge density of 424 μC cm^{-2}. This provides a convenient method to determine the electrochemical surface area (ECSA) of Pd, without the complication of surface contamination, as occurs with other methods (*e.g.*, UPD of Cu, and CO stripping).[10,22] By this method, the specific ECSA of the Pd-BP nanoparticles was estimated to be 122 m^2 g^{-1}, which is about 3.6 times higher than that of commercial Pd black (33.6 m^2 g^{-1}). This is most likely due to the smaller particle size and good dispersion on the electrode surface (Fig. 1). Based on the particle average core size (2.24 nm, Fig. 1), the theoretical ECSA of the Pd-BP nanoparticles was estimated to be 223 m^2 g^{-1}. This indicates that over 50% of the particle surface was accessible after the

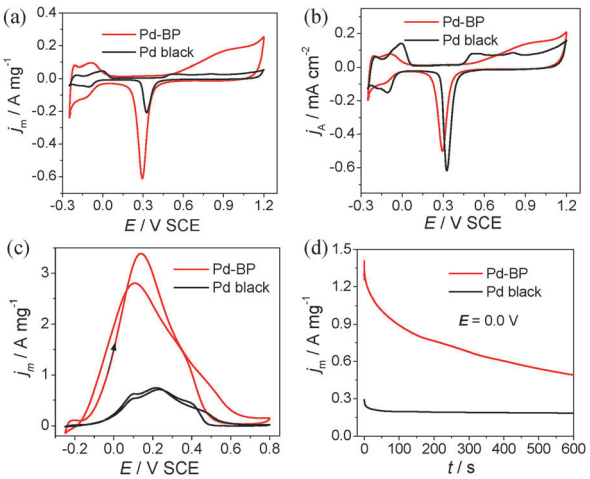

Fig. 3 Cyclic voltammograms of Pd-BP nanoparticles and commercial Pd black in 0.1 M H_2SO_4, with the currents normalized (a) by the mass loadings of Pd and (b) by the effective electrochemical surface areas at a potential scan rate of 100 mV s^{-1}. Panels (c) and (d) depict the cyclic voltammograms and current-time curves acquired at 0.0 V for HCOOH oxidation, respectively, at the Pd-BP nanoparticles and Pd black-modified electrode in 0.1 M HCOOH + 0.1 M H_2SO_4at room temperature. Pd loading on the GC electrode was 0.45 and 2.0 μg for Pd-BP and Pd black, respectively, in order to obtain similar electrochemical active areas.

particles were loaded onto the GC electrode surface. To further compare the surface characteristics, we also normalized the currents to ECSA (Fig. 3b). It can be seen that, in comparison to Pd black, the adsorption of (bi)sulfate ions at around 0 V diminished substantially on Pd-BP,[18] and the initial oxygen adsorption at around +0.50 V in the positive scan was also blocked. Such a discrepancy of surface accessibility and activity may account for the different activities in formic acid electrooxidation, as described below.

In fact, with the remarkably high ECSA, the Pd-BP nanoparticles-modified electrode exhibited a high mass activity in the electrocatalytic oxidation of formic acid. Fig. 3c depicts the voltammograms of Pd-BP and Pd black catalysts recorded in a 0.1 M HCOOH + 0.1 M H_2SO_4 solution at a potential scan rate of 100 mV s^{-1}at room temperature. In the positive scan, the peak potentials for HCOOH oxidation can be identified at +0.14 V (Pd-BP) and +0.22 V (Pd black), respectively. The negative shift (~80 mV) of the oxidation potential indicates an enhanced electrocatalytic activity of the Pd-BP nanoparticles; an important attribute in increasing the working voltage of fuel cells. More significantly, the peak current density of the Pd-BP nanoparticles is as high as 3.39 A mg^{-1}_{Pd}, which is about 4.5 times higher than that of the Pd black (0.75 A mg^{-1}). This value is also significantly higher than those reported so far for Pd/C (which are in the range 1.4–2.7 A mg^{-1}),[10,23,24] Pd nanosheets (1.38 A mg^{-1}),[25] and PtPd alloy nanoparticles (1.1 A mg^{-1}).[26]

The stability of the electrocatalysts under continuous operating conditions was further examined by chronoamperometric measurements. Fig. 3d shows the current–time curves recorded at 0.0 V for 600 s. The Pd-BP catalysts maintained a mass current density that was 2.7–4.8 times higher than that of Pd black, demonstrating significantly enhanced electrocatalytic activity and stability.

In summary, stable butylphenyl-functionalized palladium nanoparticles (core dia. 2.24 nm) were synthesized. Because of the high specific electrochemical surface area and unique surface-functionalization, the Pd-BP nanoparticles exhibited 4.5 times higher electrocatalytic activity than commercial Pd black for formic acid oxidation. The present study demonstrates that surface functionalization of precious metal nanoparticles is a promising route to the preparation of high performance fuel cell nanocatalysts.

This work was supported by the National Science Foundation (CHE-0832605 and CHE-1012258). We thank Y.-C. Hwang (UCSC) for the TEM measurements.

Notes and references

1 C. Rice, S. Ha, R. I. Masel and A. Wieckowski, *J. Power Sources*, 2003, **115**, 229–235.
2 X. W. Yu and P. G. Pickup, *J. Power Sources*, 2008, **182**, 124–132.
3 Y. W. Rhee, S. Y. Ha and R. I. Masel, *J. Power Sources*, 2003, **117**, 35–38.
4 S. Uhm, H. J. Lee, Y. Kwon and J. Lee, *Angew. Chem., Int. Ed.*, 2008, **47**, 10163–10166.
5 H. X. Zhang, C. Wang, J. Y. Wang, J. J. Zhai and W. B. Cai, *J. Phys. Chem. C*, 2010, **114**, 6446–6451.
6 A. Capon and R. Parsons, *J. Electroanal. Chem.*, 1973, **45**, 205–231.
7 S. G. Sun, J. Clavilier and A. Bewick, *J. Electroanal. Chem.*, 1988, **240**, 147–159.
8 W. P. Zhou, A. Lewera, R. Larsen, R. I. Masel, P. S. Bagus and A. Wieckowski, *J. Phys. Chem. B*, 2006, **110**, 13393–13398.
9 H. Miyake, T. Okada, G. Samjeske and M. Osawa, *Phys. Chem. Chem. Phys.*, 2008, **10**, 3662–3669.
10 W. J. Zhou and J. Y. Lee, *J. Phys. Chem. C*, 2008, **112**, 3789–3793.
11 F. J. Vidal-Iglesias, J. Solla-Gullon, E. Herrero, A. Aldaz and J. M. Feliu, *Angew. Chem., Int. Ed.*, 2010, **49**, 6998–7001.
12 H. Meng, C. Wang, P. K. Shen and G. Wu, *Energy Environ. Sci.*, 2011, **4**, 1522–1526.
13 D. Ghosh and S. W. Chen, *J. Mater. Chem.*, 2008, **18**, 755–762.
14 H. H. Yang and R. L. McCreery, *Anal. Chem.*, 1999, **71**, 4081–4087.
15 D. Lin-Vien, N. B. Colthup, W. G. Fateley and J. G. Grasselli, *The Handbook of Infrared and Raman Characteristics Frequencies of Organic Molecules*, Academic Press, New York, 1991.
16 M. J. Hostetler, J. E. Wingate, C. J. Zhong, J. E. Harris, R. W. Vachet, M. R. Clark, J. D. Londono, S. J. Green, J. J. Stokes, G. D. Wignall, G. L. Glish, M. D. Porter, N. D. Evans and R. W. Murray, *Langmuir*, 1998, **14**, 17–30.
17 C. Susut, G. B. Chapman, G. Samjeske, M. Osawa and Y. Tong, *Phys. Chem. Chem. Phys.*, 2008, **10**, 3712–3721.
18 N. Hoshi, K. Kagaya and Y. Hori, *J. Electroanal. Chem.*, 2000, **485**, 55–60.
19 H. Duncan and A. Lasia, *Electrochim. Acta*, 2008, **53**, 6845–6850.
20 H. P. Liang, N. S. Lawrence, T. G. J. Jones, C. E. Banks and C. Ducati, *J. Am. Chem. Soc.*, 2007, **129**, 6068–6069.
21 D. A. J. Rand and R. Woods, *J. Electroanal. Chem.*, 1971, **31**, 29–38.
22 L. L. Fang, Q. A. Tao, M. F. Li, L. W. Liao, D. Chen and Y. X. Chen, *Chin. J. Chem. Phys.*, 2010, **23**, 543–548.
23 M. Chen, Z. B. Wang, K. Zhou and Y. Y. Chu, *Fuel Cells*, 2010, **10**, 1171–1175.
24 N. C. Cheng, H. F. Lv, W. Wang, S. C. Mu, M. Pan and F. Marken, *J. Power Sources*, 2010, **195**, 7246–7249.
25 X. Q. Huang, S. H. Tang, X. L. Mu, Y. Dai, G. X. Chen, Z. Y. Zhou, F. X. Ruan, Z. L. Yang and N. F. Zheng, *Nat. Nanotechnol.*, 2011, **6**, 28–32.
26 E. A. Baranova, N. Miles, P. H. J. Mercier, Y. Le Page and B. Patarachao, *Electrochim. Acta*, 2010, **55**, 8182–8188.